Quantum Nondemolition Measurements of Moving Target States

Anton L. Andersen*
Center for Complex Quantum Systems, Department of Physics and Astronomy, Aarhus University, Ny Munkegade 120, DK-8000 Aarhus C, Denmark

Klaus Mølmer†
Aarhus Institute of Advanced Studies, Aarhus University, Høegh-Guldbergs Gade 6B, DK-8000 Aarhus C, Denmark and Center for Complex Quantum Systems, Department of Physics and Astronomy, Aarhus University, Ny Munkegade 120, DK-8000 Aarhus C, Denmark

(Received 21 January 2022; accepted 26 August 2022; published 14 September 2022)

We present a protocol for probing the state of a quantum system by its resonant coupling and entanglement with a meter system. By continuous measurement of a time evolving meter observable, we infer the evolution of the entangled systems and, ultimately, the state and dynamics of the system of interest. The photon number in a cavity field is thus resolved by simulated monitoring of the Rabi oscillations of a resonantly coupled two-level system, and we propose to regard this as a practical extension of quantum nondemolition measurements with applications in quantum metrology and quantum computing.

DOI: 10.1103/PhysRevLett.129.120402

Introduction.—In most studies and applications of quantum systems, it is required to perform measurements of a physical observable to detect its value in a given state or changes of its value due to physical interactions. So-called quantum nondemolition (QND) measurements employ interactions with a measurement apparatus that does not change the value of the observable of interest or any other property of the system that may subsequently cause changes of that value [1–3]. QND measurements are useful for precision monitoring of perturbations or dissipative state changes of quantum systems and sensors [3–6].

Early experiments employed the optical Kerr effect and parametric amplification to perform QND measurements on propagating light fields [7–9]. Real and artificial atoms and cavity fields permit practical detection schemes where a sequence of weak measurements accumulates measurement statistics and gradually approaches a projective measurement on the system [10–18]. Such measurements may also be used to identify infrequent quantum jumps among eigenstates [19–26]. The Hamiltonian of a quantum system constitutes a QND observable, and its energy eigenstates can be probed by dispersive interactions that perturb the energy and cause a complex phase evolution of the eigenstates of qubit or field probes. To ensure that no energy is exchanged between the system and the probe, the interactions have to be far-off resonant, and the phase evolution of the probe system, given by second order perturbation theory, is typically slow.

Probing by resonant Rabi dynamics.—In this Letter, we propose a different and faster approach to measure and monitor the energy eigenstates of a quantum system. Our proposal relies on weak continuous probing of a meter system that is subject to resonant interactions and oscillatory exchange of energy with the system of interest. We demonstrate the proposal by simulating the probing of the excited state population of a two-level system coupled to a harmonic oscillator by the Jaynes-Cummings interaction. Figures 1(a) and 1(b) recall how a mixture or superposition of oscillator eigenstates $\{|n\rangle\}$ leads to the so-called damped and revived Rabi oscillations, appearing as the weighted sum of oscillations with different n-dependent frequencies, cf., experiments with trapped ions [27] and superconducting qubits [28]. The total number of excitations shared between the probe and the oscillator is a conserved quantity, and we suggest to infer its value by measuring the oscillation frequency of the probe qubit excited state population. This can be done with a classical far-off resonant probe, and instead of the repeated projective measurements applied in [27,28], which successfully reproduce the average behavior shown in Fig. 1(a), our continuous observation concerns a single system and fluctuating rather than average values. The system is hence simulated by a stochastic master equation [29,30], and Fig. 1(c) shows how the state of the system conditioned on the measurement record develops full contrast oscillations of the probe excitation with a well resolved single frequency and a corresponding well defined value of the shared number of excitations in the system. We shall refer to this as degenerate subspace QND detection (DS QND), while noting that the oscillatory behavior in Fig. 1(c) determines both the number of excitations, and hence the pair of states $\{|n+1,g\rangle, |n,e\rangle\}$, *and* the phase of

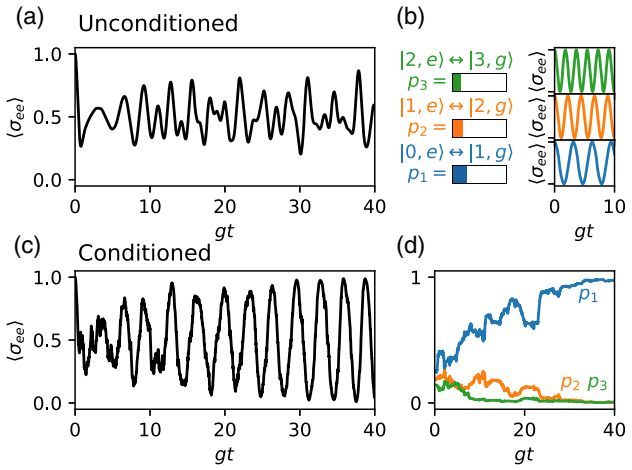

FIG. 1. (a) Unconditioned dynamics of the excited state population $\langle\hat{\sigma}_{ee}\rangle$ of a two-level system resonantly coupled to a harmonic oscillator. The complex behavior is due to its composition as a sum with weight factors p_n of regular quantum Rabi oscillations with different frequencies shown in panel (b). Panel (c) shows the stochastic dynamics of the expectation value $\langle\hat{\sigma}_{ee}\rangle$, conditioned on weak continuous measurements of $\hat{\sigma}_{ee}$ and simulated by the stochastic master equation (2). The continuous probing of $\hat{\sigma}_{ee}$ gradually identifies a single Rabi oscillation frequency and hence collapses the system from an initial thermal ensemble with mean excitation $\langle\hat{n}\rangle = 3$ into a single energy subspace as shown by the evolution of the subspace probabilities p_n in panel (d).

the oscillation, so we are, in fact, tracking a coherent superposition state, which periodically factors into an oscillator number state and a probe system energy eigenstate (at instants when $\langle\hat{\sigma}_{ee}\rangle = 0, 1$). We shall now present the theory leading to Figs. 1(c) and 1(d), and quantify the performance of DS QND.

Weak continuous measurements.—We consider a harmonic oscillator resonantly coupled to a qubit with states $|g\rangle$ and $|e\rangle$, via the resonant Jaynes-Cummings Hamiltonian,

$$H = \omega(\hat{a}^\dagger\hat{a} + \hat{\sigma}_{ee}) + g(\hat{a}^\dagger\hat{\sigma}_{ge} + \hat{a}\hat{\sigma}_{eg}), \tag{1}$$

where $\hbar = 1$ such that ω is the energy spacing of the oscillator and the qubit, $\hat{a}^\dagger$ ($\hat{a}$) is the creation (annihilation) operator of the oscillator, $\hat{\sigma}_{ij} = |i\rangle\langle j|$ and g is the coupling strength. The Jaynes-Cummings coupling drives oscillations between product states $|n,e\rangle \leftrightarrow |n+1,g\rangle$ with angular frequency $2g\sqrt{n+1}$, as seen in Fig. 1(b).

We imagine that the qubit is a real or artificial atom and that the qubit observable $\hat{\sigma}_{ee}$ can be continuously measured by phase sensitive, homodyne detection of a classical probe field coupling $|e\rangle$ off resonantly to a further excited state. While this probing occurs, the system is governed by the stochastic master equation [29,30],

$$d\rho = -i[H,\rho]dt + k\mathcal{D}[\hat{\sigma}_{ee}]\rho dt + \sqrt{2k\eta}\mathcal{H}[\hat{\sigma}_{ee}]\rho dW, \tag{2}$$

where k denotes the measurement strength and η is the measurement efficiency. The first term in Eq. (2) describes coherent Rabi oscillation dynamics. The second term in Eq. (2) contains the dissipation superoperator

$$\mathcal{D}[\hat{O}]\rho = 2\hat{O}\rho\hat{O}^\dagger - \{\hat{O}^\dagger\hat{O},\rho\}, \tag{3}$$

describing decoherence due to the disturbance caused by the measurement. The final term in Eq. (2) contains the superoperator

$$\mathcal{H}[\hat{O}]\rho = \hat{O}\rho + \rho\hat{O}^\dagger - \langle\hat{O} + \hat{O}^\dagger\rangle_\rho, \tag{4}$$

where $\langle\hat{O}\rangle_\rho = \mathrm{Tr}[\hat{O}\rho]$. This term describes the stochastic measurement backaction. The Wiener noise increment dW in Eq. (2) is given by the difference between the random measurement outcome obtained in the experiment $dY(t)$, and its expected mean value,

$$dY(t) = \langle\hat{\sigma}_{ee}\rangle_\rho dt + \frac{dW}{\sqrt{8k\eta}}. \tag{5}$$

dW represents Gaussian noise with zero mean and variance equal to dt on the phase quadrature of the probe field, and it can be simulated in numerical studies. Numerical solutions of the stochastic master equation are obtained using the QuTiP toolbox [31,32].

To observe how the continuous measurement of $\hat{\sigma}_{ee}$ reveals the oscillator dynamics, we will consider a situation where the qubit is initially prepared in the state $|e\rangle$, while the harmonic oscillator is in a mixed state described by $\rho_{HO} = \sum_n p_n(t=0)|n\rangle\langle n|$. Results of simulations are presented in Fig. 2 for $\eta = 1$, and they show that the system converges to states with a definite total number of excitations. For the case of weak probing [panels (a) and (b)], we see that the definite value of n occurs together with a definite harmonic evolution of the excited state population (at frequency $2g\sqrt{n+1}$), while intermediate probing strengths [panels (c) and (d)], identify a definite value of n faster, despite the Rabi oscillations being significantly disturbed by the measurement process. For even stronger probing [panels (e) and (f)] the coherent Rabi oscillations are replaced by infrequent jumps between the probe states, and the distinction between different values of n takes longer time. For values of the measurement efficiency $\eta < 1$ the signal-to-noise ratio is decreased, cf. Eq. (5), and the corresponding measurement backaction in Eq. (2) is reduced. The DS QND mechanism still applies but it occurs on a longer timescale.

Optimal probing strength.—In order to assess the time needed for the continuous measurements to determine the degree of excitation of the oscillator, we study the convergence toward unity of the purity $P = \mathrm{Tr}(\rho^2)$ of the conditional density matrix. As seen in Fig. 3, we can fit its mean value over many trajectories with an exponential

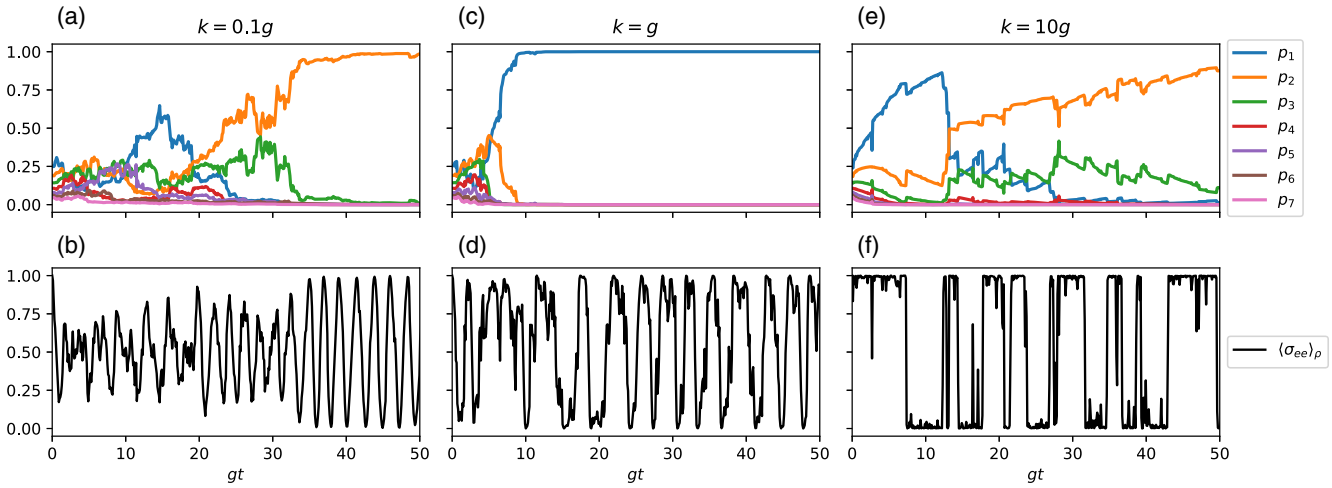

FIG. 2. Quantum trajectory simulations of the dynamics of the Jaynes-Cummings system subject to weak continuous probing [$k = 0.1g$, panels (a) and (b)], intermediate probing [$k = g$, panels (c) and (d)], and strong probing [$k = 10g$, panels (e) and (f)] of the excited state population of the two-level probe system. The harmonic oscillator is prepared initially in a thermal state with mean excitation number $\langle\hat{n}\rangle = 3$ and the qubit is prepared in the excited state. The upper panels show the conditional probabilities for the total (integer) number of excitations, while the lower panels show the qubit excited state population.

model, and repeating the procedure for different probing strengths we observe in the inset of Fig. 3 that the time needed to perform DS QND is smallest in the intermediate strength probing regime, $k \simeq g$.

This result can be explained qualitatively, since probing with a small value of k only yields an appreciable signal to noise when accumulated over times $\propto 1/k$. During that time the system undergoes one or several Rabi oscillations, and despite the white noise component in the weak probe signal it is possible to discern a single leading harmonic component and hence reveal the value of n. While increasing k increases the data extraction rate, when k becomes of the order of the value of g the backaction of the qubit excited state measurements causes significant disturbance of the Rabi oscillations. Discerning different n values by the frequency of the Rabi oscillations is gradually hampered by these disturbances when k exceeds g. Ultimately, when k is very large, the measurements effectively project the qubit in its energy eigenbasis and thus freezes the Rabi oscillations by the quantum Zeno mechanism [33], see Fig. 2(f). The moderate and strong measurement backaction does not invalidate the QND property with respect to distinction of Rabi subspaces, but they modify the harmonic population oscillation within the subspaces as shown in Fig. 2. This explains why the distinction between different subspaces eventually becomes less effective.

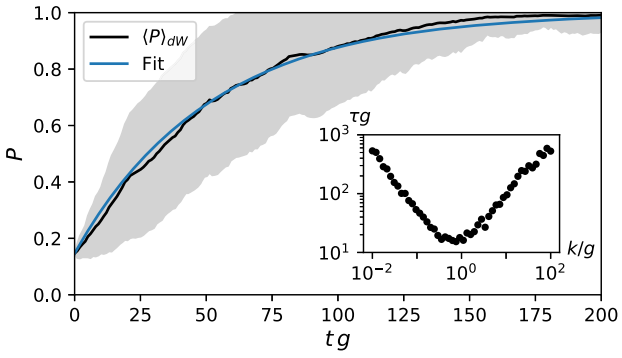

FIG. 3. The average purity $\langle P\rangle_{dW}$ of 200 simulated trajectories under weak probing ($k = 0.1g$). The shaded area represents one standard deviation from the mean. The average time τ, needed to measure the energy, is extracted by fitting the purity $P(t) = 1 - [1 - P(t = 0)]e^{-t/\tau}$. The inset shows the average time of distinction of the excitation of the harmonic oscillator, prepared with an initial thermal distribution with $\langle\hat{n}\rangle = 3$, as a function of probing strength k.

Observation of quantum jumps.—DS QND may be applied to mechanical oscillators, quantized fields, photons, and magnons, which are all systems where there has been an interest in demonstrating the quantized nature of their interactions [11–18,20,34,35], and dynamical features such as quantum jumps [19,22–26]. The latter experiments are often hampered by the time between jumps being comparable to the time needed to detect the change of n in an experiment. The time, $\sim 1/g$, needed to resolve the resonant Rabi oscillations frequencies by our method for low values of n may be much shorter than the time needed for the dispersive coupling which assumes a detuning $\delta \gg g$ and a resulting weaker coupling strength $(g^2/\delta) \ll g$. DS QND may thus be particularly useful to resolve quantum jumps, and we now discuss how to incorporate thermal quantum jumps in the formalism and present simulations of their detection from the measurements on the probe system.

If the harmonic oscillator is connected to a thermal reservoir with an average number of excitations n_T and coupling rate γ, Eq. (2) is modified into

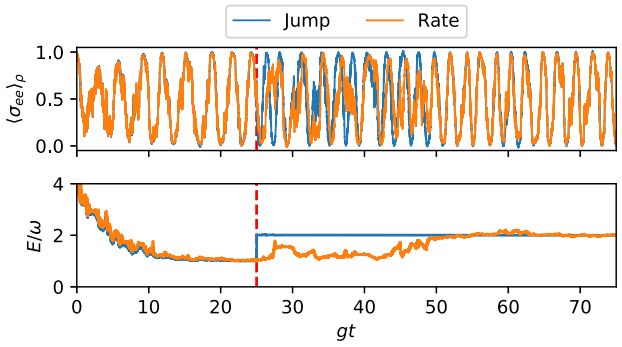

FIG. 4. Observation of a quantum jump. The orange curve in the upper (lower) panel shows the excited state population (average excitation of the oscillator) inferred from weak continuous measurements on the qubit meter. The oscillator is subject to a single quantum jump occurring at $gt = 25$, and the blue curves show the inferred qubit excited state population and oscillator number of quanta, assuming the added knowledge of when the jump happened. Parameters used for the simulation are $k = 0.1g$, $\gamma = 10^{-3}g$, and $\langle\hat{n}\rangle = n_T = 3$.

$$d\rho = -i[H,\rho]dt - \frac{\gamma}{2}(n_T+1)\mathcal{D}[\hat{a}]\rho dt - \frac{\gamma}{2}n_T\mathcal{D}[\hat{a}^\dagger]\rho dt + k\mathcal{D}[\hat{\sigma}_{ee}]\rho dt + \sqrt{2k\eta}\mathcal{H}[\hat{\sigma}_{ee}]\rho dW. \quad (6)$$

The terms involving $\mathcal{D}[\hat{a}]$ and $\mathcal{D}[\hat{a}^\dagger]$ are responsible for the loss or absorption of excitations to or from the bath.

Figure 4 shows a simulation of the dynamics described by Eq. (6). For this particular simulation, we assumed that no quanta were emitted into or absorbed from the bath until $gt = 25$ where we simulated an incoherent heating event. The blue curve in the lower panel shows the mean excitation of the oscillator, inferred by a hypothetical observer of both the probing dynamics and the occurrence of the energy exchange between the oscillator and the heat bath, while the orange curve shows the mean excitation of the oscillator inferred by an observer having only access to the continuous probing record. In the upper panel, the change in n at $t = 25/g$ accompanies a change in the Rabi oscillation frequency appearing instantly in the regular blue curve inferred by the hypothetical observer. The more erratic orange curve reveals the uncertainty of the real observer who realizes the change of state and agrees with the hypothetical observer only after the signal has accumulated to permit distinction of the different n values.

Figure 5 shows a longer measurement record with multiple jumps inferred as the rapid transfer of near unit probability weights among different values of n. As in [21,36], it is possible to use the entire measurement record and not only previous data for the theoretical estimation of the state at any given time to improve the agreement between the inferred and the true jumps in Figs. 4 and 5.

General picture.—The characteristic property of our DS QND is the convergence and subsequent restriction of the system to follow trajectories within a single degenerate

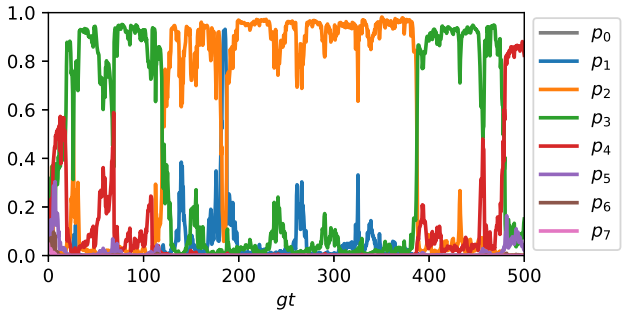

FIG. 5. Observation of multiple quantum jumps. The harmonic oscillator starts in a thermal distribution with mean excitation number $\langle\hat{n}\rangle = 3$. The probing strength $k = g$, such that it is close to the optimal value. The coupling to the bath is $\gamma = 10^{-3}g$ and its mean excitation is $n_T = 3$.

subspace of a certain operator $\hat{A}$ which commutes with the Hamiltonian, $[\hat{A},\hat{H}] = 0$. An interaction term in the Hamiltonian $\hat{H}$ causes a time evolution of a meter observable $\hat{B}$, which commutes with $\hat{A}$, and the temporal outcome of measurements of $\hat{B}$ gradually collapses the system to a definite degenerate eigenspace of $\hat{A}$. For this detection to work, it is important that the characteristic measurement records differ when the system occupies different such subspaces. In our example, $\hat{A}$ is the total number of excitations and $\hat{B}$ is the qubit meter excitation, and the Rabi oscillation frequencies, indeed, have distinct values in each eigenspace of $\hat{A}$. Notably, the measurements both reveal the degenerate subspace (of $\hat{A}$) and the actual time dependent entangled state of the system and meter within the subspace. If we assume unit measurement efficiency, and an initial mixture of pure states $|\psi_n(t)\rangle$, each occupying a single degenerate subspace of $\hat{A}$,

$$\rho(t) = \sum_n p_n(t)|\psi_n(t)\rangle\langle\psi_n(t)|, \quad (7)$$

we may generalize (2) to the measured observable $\hat{B}$

$$d\rho = -i[H,\rho]dt + k\mathcal{D}[\hat{B}]\rho dt + \sqrt{2k}\mathcal{H}[\hat{B}]\rho dW. \quad (8)$$

The ansatz in Eq. (7) then leads to the following equations:

$$dp_n = \sqrt{8k}p_n(\langle\psi_n(t)|\hat{B}|\psi_n(t)\rangle - \langle\hat{B}\rangle_{\rho(t)})dW, \quad (9)$$

and we observe that, if only one state $|\psi_n\rangle$ is populated, $p_n = 1$, $\langle\psi_n|\hat{B}|\psi_n\rangle = \langle\hat{B}\rangle_\rho$, and the stochastic noise terms do not affect the future evolution of the unit value of $p_n(t)$, while the state $|\psi_n(t)\rangle$ may still evolve within the given occupied subspace.

To further understand why the system collapses on a single subspace, we note that the purity of the system is $P(t) = \sum_n p_n^2(t)$, and applying Itô's rule for $d(p_n^2)$ yields

$$dP = \sum_n [8kp_n^2(\langle\psi_n|\hat{B}|\psi_n\rangle - \langle\hat{B}\rangle_\rho)^2 dt + \sqrt{32k}p_n^2(\langle\psi_n|\hat{B}|\psi_n\rangle - \langle\hat{B}\rangle_\rho)dW]. \quad (10)$$

The average of dW is zero and hence the average evolution of the purity obeys

$$d\langle P\rangle_{dW} = \sum_n 8k\langle p_n^2(\langle\hat{B}\rangle_n - \langle\hat{B}\rangle_\rho)^2\rangle_{dW} dt, \quad (11)$$

which is positive and causes $\langle P\rangle_{dW}$ to increase until the time evolution of $\langle\hat{B}\rangle_\rho$ is indistinguishable from the one in just one of the subspaces $\langle\hat{B}\rangle_n$. If several subspaces display the same evolution, they are not distinguished and our measurement only distinguishes their union from other subspaces with other evolution properties. While our analysis used the example of system and meter entangled state dynamics, the method is not restricted to bipartite quantum systems. The commutator requirements between $\hat{H}$ and $\hat{A}$ and between $\hat{A}$ and $\hat{B}$ suffice for our scheme to resolve the value of $\hat{A}$ for any multilevel quantum system with nontrivial eigensubspaces that can be distinguished by the continuous measurement of $\hat{B}$.

Conclusion and outlook.—We have presented a new principle for continuous QND measurements which does not project the system on the eigenstate of the QND observable but rather on a superposition state persistently evolving within a specific subspace. Different subspaces are discerned by the characteristic frequency of evolution of the mean value of an observed quantity, which may be monitored faster than the accumulation of dispersive phase shifts in the more usual QND setting.

Let us finally point to similarities between our Letter and a process referred to as emergent QND measurements [35,37]. This method probes a physical observable very weakly and, averaged over time, it determines its expectation value in one of the (nondegenerate) energy eigenstates and hence also identifies that state in a QND-like manner. Another variant of QND measurements is formed by brief position measurements carried out around times $t_n = n\pi/\omega$ of an harmonic oscillator with frequency ω [38–40], to enable the measurement of nonconserved but periodically evolving properties of quantum systems. Joint or sequential applications of these different approaches in combination with DS QND measurements may form interesting schemes to monitor quantum dynamics of more complex systems in real time and to use measurements for rapid state control.

The authors acknowledge support from the Danish National Research Foundation (Grant Agreement No. DNRF156), the European QuantERA Grant C'MON-QSENS! (Innovation Fund Denmark Grant No. 9085-00002), and the European Union's Horizon 2020 Research and Innovation Programme under the Marie Skłodowska-Curie program (754513). K. M. acknowledges discussions with Dr. Faezeh Pirmoradian in the early stages of the project.

*anton.andersen@phys.au.dk
†klaus.molmer@nbi.ku.dk

[1] V. B. Braginsky, Y. I. Vorontsov, and K. S. Thorne, Quantum nondemolition measurements, Science **209**, 547 (1980).
[2] C. M. Caves, K. S. Thorne, R. W. P. Drever, V. D. Sandberg, and M. Zimmermann, On the measurement of a weak classical force coupled to a quantum-mechanical oscillator. I. Issues of principle, Rev. Mod. Phys. **52**, 341 (1980).
[3] V. B. Braginsky and F. J. Khalili, Gravitational wave antenna with QND speed meter, Phys. Lett. **147A**, 251 (1990).
[4] V. B. Braginskii and F. I. Khalili, Frequency-anticorrelated quantum states, Zh. Eksp. Teor. Fiz. **94**, 151 (1988) [Sov. Phys. JETP **67**, 84 (1988)].
[5] V. B. Braginsky and F. Y. Khalili, Quantum nondemolition measurements: The route from toys to tools, Rev. Mod. Phys. **68**, 1 (1996).
[6] M. F. Bocko and R. Onofrio, On the measurement of a weak classical force coupled to a harmonic oscillator: Experimental progress, Rev. Mod. Phys. **68**, 755 (1996).
[7] M. D. Levenson, R. M. Shelby, M. Reid, and D. F. Walls, Quantum Nondemolition Detection of Optical Quadrature Amplitudes, Phys. Rev. Lett. **57**, 2473 (1986).
[8] P. Grangier, J. F. Roch, and S. Reynaud, Quantum correlations and non-demolition measurements using two-photon non-linearities in optical cavities, Opt. Commun. **72**, 387 (1989).
[9] P. Grangier, A. Levenson, and J.-P. Poizat, Quantum non-demolition measurements in optics, Nature (London) **396**, 537 (1998).
[10] M. Brune, P. Nussenzveig, F. Schmidt-Kaler, F. Bernardot, A. Maali, J. M. Raimond, and S. Haroche, From Lamb Shift to Light Shifts: Vacuum and Subphoton Cavity Fields Measured by Atomic Phase Sensitive Detection, Phys. Rev. Lett. **72**, 3339 (1994).
[11] B. R. Johnson, M. D. Reed, A. A. Houck, D. I. Schuster, L. S. Bishop, E. Ginossar, J. M. Gambetta, L. DiCarlo, L. Frunzio, S. M. Girvin, and R. J. Schoelkopf, Quantum non-demolition detection of single microwave photons in a circuit, Nat. Phys. **6**, 663 (2010).
[12] D. Lachance-Quirion, Y. Tabuchi, S. Ishino, A. Noguchi, T. Ishikawa, R. Yamazaki, and Y. Nakamura, Resolving quanta of collective spin excitations in a millimeter-sized ferromagnet, Sci. Adv. **3**, e160315 (2017).10.1126/sciadv.1603150
[13] T. Neuman, D. S. Wang, and P. Narang, Nanomagnonic Cavities for Strong Spin-Magnon Coupling and Magnon-Mediated Spin-Spin Interactions, Phys. Rev. Lett. **125**, 247702 (2020).
[14] K. J. Satzinger, Y. P. Zhong, H. S. Chang, G. A. Peairs, A. Bienfait, M.-H. Chou, A. Y. Cleland, C. R. Conner, É. Dumur, J. Grebel, I. Gutierrez, B. H. November, R. G. Povey, S. J. Whiteley, D. D. Awschalom, D. I. Schuster, and A. N. Cleland, Quantum control of surface acoustic-wave phonons, Nature (London) **563**, 661 (2018).

[15] Y. Chu, P. Kharel, T. Yoon, L. Frunzio, P. T. Rakich, and R. J. Schoelkopf, Creation and control of multi-phonon Fock states in a bulk acoustic-wave resonator, Nature (London) **563**, 666 (2018).
[16] P. Arrangoiz-Arriola, E. A. Wollack, Z. Wang, M. Pechal, W. Jiang, T. P. McKenna, J. D. Witmer, R. Van Laer, and A. H. Safavi-Naeini, Resolving the energy levels of a nanomechanical oscillator, Nature (London) **571**, 537 (2019).
[17] L. R. Sletten, B. A. Moores, J. J. Viennot, and K. W. Lehnert, Resolving Phonon Fock States in a Multimode Cavity with a Double-Slit Qubit, Phys. Rev. X **9**, 021056 (2019).
[18] D. Lachance-Quirion, S. P. Wolski, Y. Tabuchi, S. Kono, K. Usami, and Y. Nakamura, Entanglement-based single-shot detection of a single magnon with a superconducting qubit, Science **367**, 425 (2020).
[19] S. Gleyzes, S. Kuhr, C. Guerlin, J. Bernu, S. Deléglise, U. Busk Hoff, M. Brune, J.-M. Raimond, and S. Haroche, Quantum jumps of light recording the birth and death of a photon in a cavity, Nature (London) **446**, 297 (2007).
[20] C. Guerlin, J. Bernu, S. Deléglise, C. Sayrin, S. Gleyzes, S. Kuhr, M. Brune, J.-M. Raimond, and S. Haroche, Progressive field-state collapse and quantum non-demolition photon counting, Nature (London) **448**, 889 (2007).
[21] T. Rybarczyk, B. Peaudecerf, M. Penasa, S. Gerlich, B. Julsgaard, K. Mølmer, S. Gleyzes, M. Brune, J. M. Raimond, S. Haroche, and I. Dotsenko, Forward-backward analysis of the photon-number evolution in a cavity, Phys. Rev. A **91**, 062116 (2015).
[22] R. Vijay, D. H. Slichter, and I. Siddiqi, Observation of Quantum Jumps in a Superconducting Artificial Atom, Phys. Rev. Lett. **106**, 110502 (2011).
[23] A. Delteil, W. B. Gao, P. Fallahi, J. Miguel-Sanchez, and A. Imamoğlu, Observation of Quantum Jumps of a Single Quantum Dot Spin Using Submicrosecond Single-Shot Optical Readout, Phys. Rev. Lett. **112**, 116802 (2014).
[24] Z. K. Minev, S. O. Mundhada, S. Shankar, P. Reinhold, R. Gutiérrez-Jáuregui, R. J. Schoelkopf, M. Mirrahimi, H. J. Carmichael, and M. H. Devoret, To catch and reverse a quantum jump mid-flight, Nature (London) **570**, 200 (2019).
[25] S. Peil and G. Gabrielse, Observing the Quantum Limit of an Electron Cyclotron: QND Measurements of Quantum Jumps between Fock States, Phys. Rev. Lett. **83**, 1287 (1999).
[26] L. Sun, A. Petrenko, Z. Leghtas, B. Vlastakis, G. Kirchmair, K. M. Sliwa, A. Narla, M. Hatridge, S. Shankar, J. Blumoff, L. Frunzio, M. Mirrahimi, M. H. Devoret, and R. J. Schoelkopf, Tracking photon jumps with repeated quantum non-demolition parity measurements, Nature (London) **511**, 444 (2014).
[27] D. M. Meekhof, C. Monroe, B. E. King, W. M. Itano, and D. J. Wineland, Generation of Nonclassical Motional States of a Trapped Atom, Phys. Rev. Lett. **76**, 1796 (1996).
[28] M. Hofheinz, E. M. Weig, M. Ansmann, R. C. Bialczak, E. Lucero, M. Neeley, A. D. O'Connell, H. Wang, J. M. Martinis, and A. N. Cleland, Generation of Fock states in a superconducting quantum circuit, Nature (London) **454**, 310 (2008).
[29] Howard M. Wiseman and G. J. Milburn, *Quantum Measurement and Control* (Cambridge University Press, Cambridge, England, 2010).
[30] R. Blattmann and K. Mølmer, Conditioned quantum motion of an atom in a continuously monitored one-dimensional lattice, Phys. Rev. A **93**, 052113 (2016).
[31] J. R. Johansson, P. D. Nation, and F. Nori, QuTiP: An open-source Python framework for the dynamics of open quantum systems, Comput. Phys. Commun. **183**, 1760 (2012).
[32] J. R. Johansson, P. D. Nation, and F. Nori, QuTiP 2: A PYTHON framework for the dynamics of open quantum systems, Comput. Phys. Commun. **184**, 1234 (2013).
[33] L. S. Schulman, Continuous and pulsed observations in the quantum Zeno effect, Phys. Rev. A **57**, 1509 (1998).
[34] A. D. O'Connell, M. Hofheinz, M. Ansmann, R. C. Bialczak, M. Lenander, E. Lucero, M. Neeley, D. Sank, H. Wang, M. Weides, J. Wenner, J. M. Martinis, and A. N. Cleland, Quantum ground state and single-phonon control of a mechanical resonator, Nature (London) **464**, 697 (2010).
[35] L. Dellantonio, O. Kyriienko, F. Marquardt, and A. S. Sørensen, Quantum nondemolition measurement of mechanical motion quanta, Nat. Commun. **9**, 3621 (2018).
[36] S. Gammelmark, B. Julsgaard, and K. Mølmer, Past Quantum States of a Monitored System, Phys. Rev. Lett. **111**, 160401 (2013).
[37] D. Yang, C. Laflamme, D. V. Vasilyev, M. A. Baranov, and P. Zoller, Theory of a Quantum Scanning Microscope for Cold Atoms, Phys. Rev. Lett. **120**, 133601 (2018).
[38] G. Vasilakis, V. Shah, and M. V. Romalis, Stroboscopic Backaction Evasion in a Dense Alkali-Metal Vapor, Phys. Rev. Lett. **106**, 143601 (2011).
[39] G. Vasilakis, H. Shen, K. Jensen, M. Balabas, D. Salart, B. Chen, and E. S. Polzik, Generation of a squeezed state of an oscillator by stroboscopic back-action-evading measurement, Nat. Phys. **11**, 389 (2015).
[40] A. C. J. Wade, J. F. Sherson, and K. Mølmer, Squeezing and Entanglement of Density Oscillations in a Bose-Einstein Condensate, Phys. Rev. Lett. **115**, 060401 (2015).